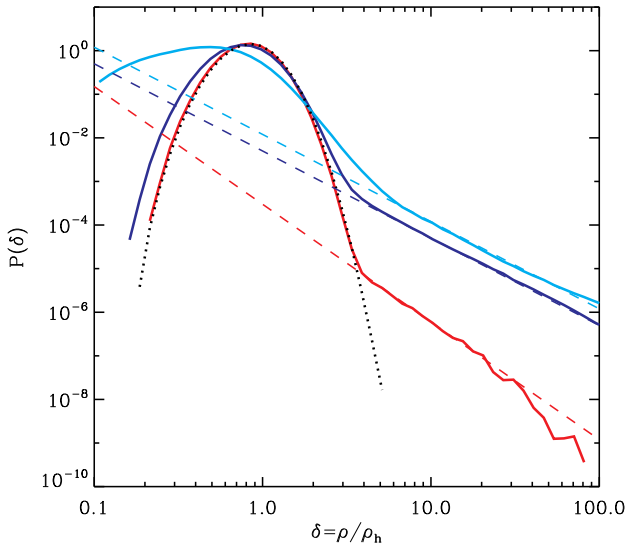

FIG. 1. The probability distribution function $P(\delta)$ obtained from simulations. The solid curves are the simulation results at $r = 300, 100$ and 10 kpc (from top to bottom). The dashed curves show our analytic approximations to the power law tail. The dotted curve indicates the contribution to the finite width of the smooth component at 10 kpc from Poisson fluctuations due to the use of $N = 32$ neighbors in the density estimator. Note that the mean host halo density ρ_h to which the x axis is normalized is $\sim 175\times$ ($\sim 4900\times$) smaller for the 100-kpc (300-kpc) curve than in the 10-kpc curve.

and the median density $\bar{\rho}$ is obtained from all the particles in that ellipsoidal shell. These δ_i are then binned in equally-spaced bins in $\log_{10}(\delta)$. In each of these bins, we calculate $P(\log_{10}\delta) = \sum_i \delta_i^{-1}$ where the sum is over all particles in that bin; the δ_i^{-1} weighting gives a volume-fraction distribution. The distribution in $\log_{10}\delta$ is then converted to a distribution in δ and normalized.

A. Power-Law Tail

The central features of Fig. 1 relevant here are the high-density power-law tails predicted by Ref. [15] (and seen already in simulations [16]). The figure shows that the amplitude of the high-density power-law tail is larger at larger radii. This can be attributed largely to the fact that the mean density $\bar{\rho}$ is ~ 175 times lower at 100 kpc than at 10 kpc, and another factor ~ 30 times lower at 300 kpc, and so the ratio of the density in substructures to the mean density is higher at larger radii.

We now use this simulation to calibrate the analytic model at a variety of radii r, from 4 to 300 kpc. At each radius we fit for the power law parameters α and f_s. We find that at radii greater than ~ 20 kpc, the smooth-halo fraction is well approximated by

$$1 - f_s(r) = 7 \times 10^{-3} \left(\frac{\bar{\rho}(r)}{\bar{\rho}(r = 100\,\mathrm{kpc})} \right)^{-0.26} . \qquad (4)$$

Note that at radii less than ~ 20 kpc, $1 - f_s(r)$ drops faster than Eq. (4); for example, $1 - f_s(10\,\mathrm{kpc}) = 4 \times 10^{-4} \approx 1.5\times10^{-3}\,(\bar{\rho}(10\,\mathrm{kpc})/\bar{\rho}(100\,\mathrm{kpc}))^{-0.26}$. This close to the center, however, the clumpiness of the simulated halo is likely artifically suppressed due to finite resolution effects. The best-fit values of α are 0.0 ± 0.1 at all radii greater than 20 kpc. In the following, we implicitly assume $\alpha = 0$ and the radial dependence in f_s given by Eq. (4).

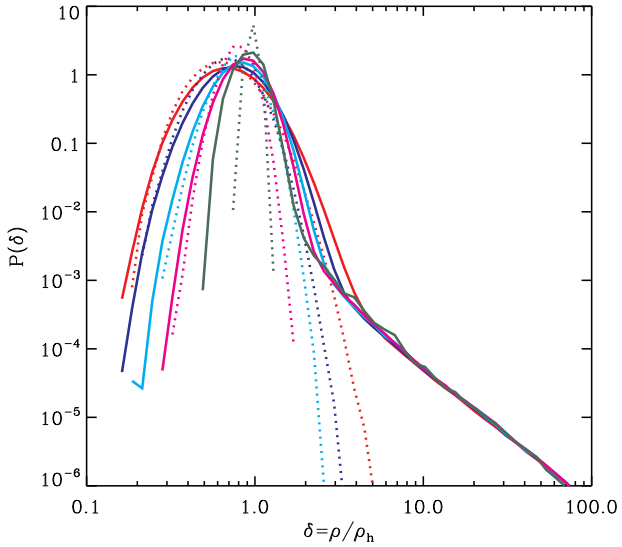

FIG. 2. The probability distribution function $P(\delta)$ at 100 kpc for particle densities estimated from the nearest $N = (16, 32, 64, 128, 1024)$ neighbors.

B. Finite Width of the Smooth Component

The simulation results shown in Fig. 1 show a finite width Δ for the smooth component. However, care must be taken as Poisson fluctuations due to the finite number N of nearest neighbors in the density estimator will also contribute to the width. In Fig. 2 we show $P(\delta)$ at 100 kpc for densities determined with $N = 16$, 32, 64, 128, and 1024. The dotted curves indicated the expected contribution to the width from Poisson fluctuations (and note that the true and Poisson widths should add in quadrature), which we obtained by running the density estimator on a randomly distributed sample of 10^6 particles. As N is increased, the width of the smooth component decreases, but not quite as fast as the Poisson fluctuations, and by $N = 1024$ it is clear that the true width has been resolved to be about $\Delta \simeq 0.2$. At 10 kpc